



HAL
open science

Indentation cracking in mono and polycrystalline cubic zirconia: Methodology of an apparent fracture toughness evaluation

Ronan Henry, Nathalie Le Roux, Isabelle Zacharie-Aubrun, Jean-Marie Gatt, Cyril Langlois, Sylvain Meille

► **To cite this version:**

Ronan Henry, Nathalie Le Roux, Isabelle Zacharie-Aubrun, Jean-Marie Gatt, Cyril Langlois, et al.. Indentation cracking in mono and polycrystalline cubic zirconia: Methodology of an apparent fracture toughness evaluation. *Materials Science and Engineering: A*, 2022, 860, pp.144261. 10.1016/j.msea.2022.144261 . hal-03844422

HAL Id: hal-03844422

<https://hal.science/hal-03844422>

Submitted on 8 Nov 2022

HAL is a multi-disciplinary open access archive for the deposit and dissemination of scientific research documents, whether they are published or not. The documents may come from teaching and research institutions in France or abroad, or from public or private research centers.

L'archive ouverte pluridisciplinaire **HAL**, est destinée au dépôt et à la diffusion de documents scientifiques de niveau recherche, publiés ou non, émanant des établissements d'enseignement et de recherche français ou étrangers, des laboratoires publics ou privés.

Indentation cracking in mono and polycrystalline cubic zirconia: methodology of an apparent fracture toughness evaluation

Ronan Henry ^{a,b}, Nathalie Le Roux ^a, Isabelle Zacharie-Aubrun ^b, Jean-Marie Gatt ^b, Cyril Langlois ^a, Sylvain Meille ^{*a}

^a Univ Lyon, INSA Lyon, UCBL, CNRS, MATEIS, UMR5510, 69621 Villeurbanne, France

^b CEA, DEN, DEC, St. Paul Lez Durance 13108, France

* Corresponding author, sylvain.meille@insa-lyon.fr

Keyword

Indentation, cracking, microstructure, fracture toughness, ceramics

Abstract

Indentation-induced cracking with sharp tips is studied on mono- and polycrystalline cubic zirconia. Tests at different applied loads are carried out, ranging below and above a threshold load above which visible surface cracking is noted after testing. This threshold load does not appear to be correlated to any discontinuity in the evolution of either the hardness or the irreversible energy ratio with applied load. The crystal orientation and the presence of grain boundaries clearly affects the shape of the cracks generated around the residual imprint. Polycrystalline samples show significantly shorter indentation induced cracks and therefore a higher apparent toughness than single crystals for the same load. In addition, for single crystals, cracks are deflected towards {110} type planes, appearing to be the most susceptible to cracking, and thus logically presenting the lowest apparent toughness. Tests with a Berkovich tip leads to an average of different crystal orientations, while tests with a Vickers tip can be used to test a specific crystal orientation in the case of a cubic crystal such as zirconia.

1. Introduction

Indentation testing is frequently used to determine the fracture toughness of brittle materials. This testing method was originally based on Hertz's work on contact mechanics [1], which describes the elastic contact between two solids, at the origin of the analysis of indentation testing with spherical tips [2]. Subsequently, pyramidal tips became widely used [3], as the technique is economical, easy to use and versatile [4]. The tip generates an elastic - plastic deformation, in the shape of a quasi-half-sphere, under the impression [5]. The study of the cracks induced by indentation was initiated by Palmqvist in 1957 [6], but the measurement of the fracture toughness of the material by the characterization of the length of the surface cracks was first proposed by Evans and Charles in 1976 [7]. This technique appeared then as a very attractive method for measuring toughness, illustrated by numerous research works on the subject. It is often referred to as *IF* (or *VIF*) for (Vickers) Indentation Fracture toughness test.

This method to measure fracture toughness has been challenged in the last decades notably by Quinn and Bradt [8]. They point out the large number of equations available in the literature to calculate the fracture toughness, mentioning that this presages a lack of theoretical basis. The measured stress intensity factor is also more a criterion for crack arrest than for crack propagation. However, this method is based on well-documented fracture mechanics for model cracks systems [4]. Even if the fracture toughness measurement is subjected to uncertainties of up to 40%, it remains a fast, efficient and easy method for exploratory testing in the field of fracture mechanics. Thus, it is particularly suitable for comparative measurements and for testing small elements inaccessible by other techniques.

The local measurement of fracture parameters can be particularly attractive for example for a fragmented ceramic whose intrinsic properties have to be determined, such as irradiated nuclear fuel [9]. Alternatives to instrumented indentation exist, for instance by preparing and testing micrometric specimens [10], but this requires much more time and more complex equipment. However, the use of indentation testing raises questions, in particular with regard to the accuracy of fracture toughness measurements [8]. Due to the brittleness of ceramic materials, indentation tests on ceramics are almost inevitably associated with the formation of cracks [11], either micro-cracks, which are not visible on the surface, or larger cracks which extend up to the surface. Nano-indentation at low applied loads, typically below 100 mN for sharp tips, works particularly well for determining the hardness H of ceramics because the applied load is not high enough to form cracks [12]. However, for micro-indentation tests with a load above 100 mN, cracks form around the indent, leading to larger uncertainties in the measurement of H [13], a parameter needed for fracture toughness determination. Typically, indentation testing at the scale of a single grain, or of a few grains, raises the question of the effect of local non-homogeneities (crystal anisotropy, grains boundaries...) on the measured parameters (hardness H and Young's modulus E) but also on the cracking system and thus on the measured apparent stress intensity factor.

The aim of this work is to study the influence of the local microstructure on the fracture behavior studied by indentation testing on a brittle material with known properties (8Y-FSZ cubic zirconia). For this purpose, different parameters are studied (crack shape and length, hardness H , indentation energy W) in different configurations (polycrystalline samples, monocrystalline samples tested in distinct crystalline orientations) and for different indentation tips. In order to observe the effect of cracking on the measured indentation parameters, the study was carried out with a large applied load range including both crack-free tests and tests associated with cracks propagation.

2. Experimental procedure

2.1. Materials

The material of interest is 8Y-FSZ zirconia (fully stabilized in cubic phase with 8%mol of Ytria). Two different samples were used.

The first sample is a polycrystalline *8Y-FSZ* (Microcertec, Collegien, France) in the shape of a pellet of 8 mm in diameter and 2 mm in thickness. Grains have an average equivalent diameter of $6.5 \pm 3.1 \mu\text{m}$ and the sample has a porosity fraction of $2.1 \pm 0.5\%$.

The second sample is a dense monocrystalline *8Y-FSZ* sample (MSE Supplies, Tucson, USA). This single crystal is a square cuboid of $10 \times 10 \times 0.5 \text{ mm}^3$, with its upper surface being a {100} crystalline plane. In order to determine precisely the crystalline orientation of the single crystal, an EBSD (Electron Backscatter Diffraction) map was acquired using a NordlysII fast camera and Aztec software (Oxford Instruments, Abingdon-on-Thames, UK) in a SEM Supra55VP (Carl Zeiss, Oberkochen, Germany).

Both samples were mechanically polished firstly with diamond suspensions down to $1 \mu\text{m}$ and finally with a vibratory polishing using colloidal silica of average particles size of $0.03 \mu\text{m}$.

2.2. Testing setups

Indentation tests were performed at room temperature with a nanoindenter G200 (Keysight Technologies, Santa Rosa, USA). Two indentation tips were used: Berkovich (three-sided pyramid) and Vickers (four-sided pyramid). Tests were carried out by force driving up to the maximum load P at a strain-rate $\dot{\epsilon}$ of 0.05 s^{-1} defined as $\dot{\epsilon} = \frac{1}{P} \frac{dP}{dt}$ and with a 10 s holding time at the maximum load. Several tests were carried out at a dozen different applied loads between 20 mN and 660 mN. For each load, ten tests were performed on polycrystalline samples and three tests on monocrystalline sample, as the microstructure is more homogenous and data is less scattered in that case.

Samples were fixed to a rigid sample holder which can be rotated into the indentation system, allowing the orientation of the single crystal relatively to the indenter tip. The sample is rotated manually, but the rotation angle is precisely measured on the optical microscope used for indentation localization. As the sample surface is a {100} crystalline plane, some {100} and {110} planes are normal to the sample surface and can be targeted by indentation induced cracks by aligning the diagonal impression with $\langle 100 \rangle$ and $\langle 110 \rangle$ directions respectively. On the other hand, {111} planes are not available, because they are not perpendicular to the sample surface.

In the present article, the so called “{100} orientation” or “{110} orientation” corresponds to a crystal rotation for which a {100} or a {110} plane is perpendicular to the sample surface and one diagonal of the indentation tip points towards this plane. When a Berkovich tip is used in such a case, only one diagonal of the tip is aiming the crystalline plane, the two other diagonals being in a random orientation. However, when a Vickers tip is used, each of the four diagonals is aiming the same family type of plane. A “{NS} (Non-Specific) orientation” is also tested and does not test any specific crystal plane.

Every residual indentation impression was imaged using both electronic and optical microscopy. Electronic imaging was performed by a SEM Supra55VP (Carl Zeiss, Oberkochen, Germany), using a low current of 0.5 kV in order to reduce charging effects. Optical imaging (Axiophot Carl Zeiss, Oberkochen, Germany) was performed at a magnification of $\times 625$.

2.3. Parameters determination

Hardness H is generally defined by the ratio of the applied load P to the projected contact area A of the indentation imprint, which depends on the contact depth h_c following equation (1):

$$H = \frac{P}{A(h_c)} \quad (1)$$

For a perfect Berkovich or Vickers pyramidal tip, $A(h_c) = 24.5 h_c^2$. However, as the tip ending can be non-perfect, a calibration of the tips was performed. The contact area $A(h_c)$ was defined by a 5-parameter polynomial function and was fitted by performing tests on fused silica over the load range used in this study, *i.e.* up to 650 mN.

The Young's modulus was estimated by the Oliver and Pharr analysis [14] based on the slope of the beginning of the unloading curve considering a Poisson's ratio of 0.3.

On brittle materials, such as the cubic zirconia used in this work, two main cracking systems are commonly considered around the residual indentation impression: radial (type P or Palmqvist) and median (type M or Half-Penny) (**FIGURE 1**) [15]. However, intermediate states exist, such as radial-median system or lateral cracks that develop under the sample surface.

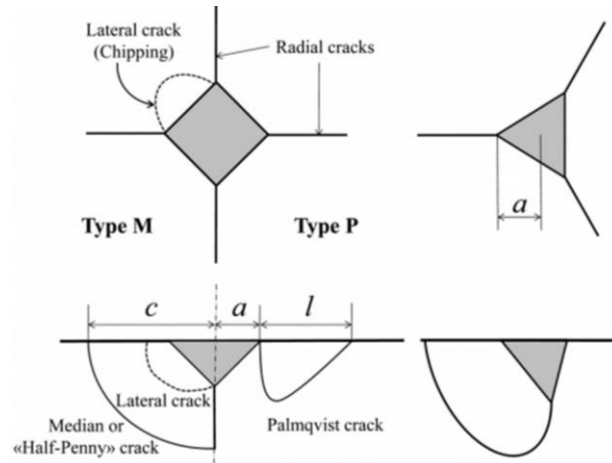


Figure 1: Schematics of indentation impressions and cracks [16] (top: surface view, bottom : section view) and their associated parameters on (left) Vickers, (right) Berkovich indenters. The grey area is the surface of residual impression A .

Many different equations exist to calculate the apparent fracture toughness depending on the cracking system generated, but also on the geometry of the tip [17][18]. Most of them are derived from the analysis of cracks generated at the interface of a plastic zone and an elastic zone in a solid, assuming half-penny shapes as developed by Lawn *et al.* [19]. These equations can be put into a generic form as described by equation (2) with variable coefficients ξ_R and n , and with P the load applied during the test, c the sum of crack length l and half diagonal of the residual impression a (**FIGURE 1**), E the Young's modulus of the tested material and H its hardness.

$$K_c = \xi_R \left(\frac{E}{H} \right)^n \frac{P}{c^{3/2}} \quad (2)$$

The most widely used equation has been proposed by Anstis [20] and is the result of a robust calibration on brittle materials (amorphous, monocrystalline and polycrystalline). It is described by $n = \frac{1}{2}$ and $\xi_R = 0.016$ for cracks in a half-penny configuration and for a Vickers tip.

Laugier *et al.* [21] adapted Anstis's equation for the Palmqvist crack configuration, with a different generic equation (3). This formalism is particularly applied to Berkovich tests because that tip has a geometry that does not allow the generated cracks in the corners to join under the impression and form a half-disc. In general, the mode of cracking assumed for Berkovich tests is the Palmqvist mode [22] and this assumption was verified by FIB tomography of the cracking system on brittle materials [23]. Dukino *et al.* fitted the Laugier equation and obtained Eq. 3 with $\chi_v = 0.016$ [22] :

$$K_C = \chi_v \left(\frac{a}{l}\right)^{1/2} \left(\frac{E}{H}\right)^{2/3} \frac{P}{c^{3/2}} \quad (3)$$

The indentation parameters, namely the half diagonal of the residual imprint a and the crack length l (**FIGURE 1**), were measured on SEM images. Each parameter is the average of the three (Berkovich tip) or four (Vickers tip) measurements. Moreover, on the single crystal tested with a Berkovich tip, when a $\{100\}$ or $\{110\}$ plane perpendicular to the surface is targeted, a and l were not averaged but only measured at the corner tip corresponding to the targeted crystalline plane (crack from others corners following different crystalline plane).

Mechanical work of indentation is determined as the area below the load-displacement curve (**FIGURE 2**). The area below the loading curve corresponds to the irreversible work W_{irr} of indentation: it is the energy lost in non-recoverable processes such as plasticity and cracking. The area below the unloading curve represents the elastic and recoverable part of indentation work W_{elas} . The sum of these two energies is the total energy W_{tot} spent during the indentation test [24].

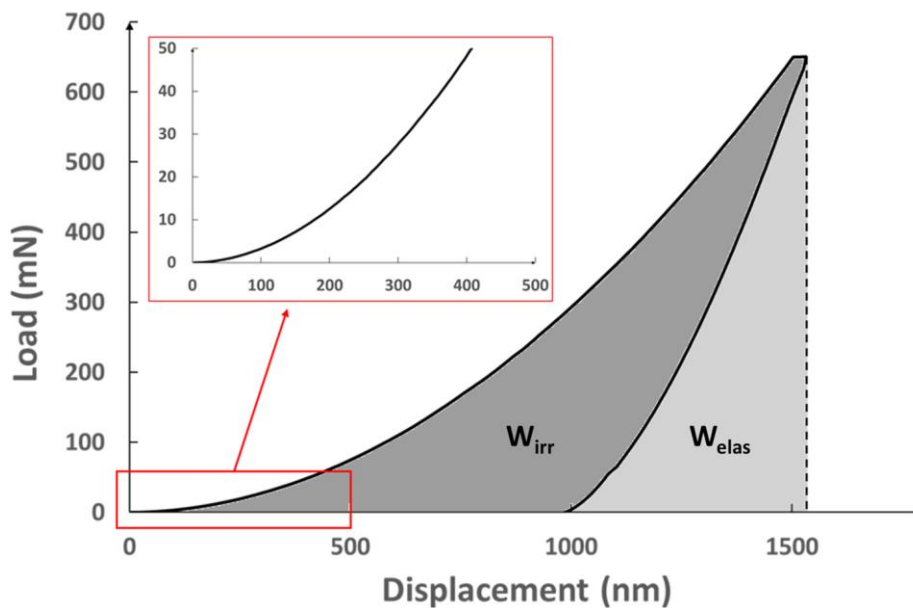


Figure 2: Example of force-displacement curve obtained by nano-indentation (here Berkovich tip up to 650 mN on polycrystalline zirconia). Calculation scheme of the indentation energy associated with the test.

3. Results

3.1. Indentation parameters

The indentation parameters measured on mono- and poly-crystalline samples with different indentation tips are given in Appendix. P is the applied load, H is the hardness, E is the Young's modulus, c is the crack length, a is the diagonal of the indentation imprint and W_{irr}/W_{tot} is the irreversible energy ratio.

3.2. Crack patterns and crack length

In this work, the cracking threshold P_{th} is defined as the lowest applied load for which a crack is systematically visible at the surface in each corner of the indentation impression. This threshold load depends on the sample but also on the tip used.

In the polycrystalline 8Y-FSZ sample, for applied loads higher than P_{th} , the Vickers tip leads to the formation of several cracks around the indentation impression, with more than one crack in each corner (FIGURE 3-A). Tests with a Berkovich tip leads to a less chaotic cracking system, with only one crack in each corner and these cracks are well aligned with the diagonals of the impression (FIGURE 3-B).

In single crystal and for both Berkovich and Vickers tips, cracking systems are very close to the theoretical models (FIGURE 1) and cracks are particularly straight and aligned with the diagonal of the imprint (FIGURE 3-C/D). As this work intends to determine the apparent fracture toughness, we did not consider the Vickers experiments on polycrystalline samples, since they produced too chaotic indentation cracks.

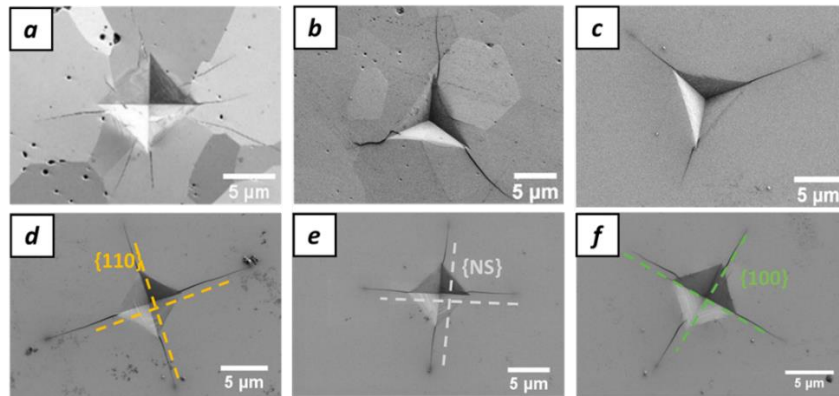


Figure 3: SEM pictures of indentation impressions: (a) Vickers on polycrystalline zirconia (650 mN), (b) Berkovich on polycrystalline zirconia (575 mN), (c) Berkovich on monocrystalline zirconia (400 mN), (d), (e), (f) Vickers on monocrystalline zirconia (400 mN), respectively on {110} orientation, {NS} (non-specific) orientation, and {100} orientation.

Using a Vickers tip is particularly efficient to test {100} and {110} planes since in the studied configuration of the single cubic crystal, these crystalline family planes have a square symmetry and some planes are perpendicular to the sample surface. Hence, with the proper sample rotation, the corners of the residual imprint are oriented towards a {100} or a {110} plane and each corner creates a crack in the same type of plane (FIGURE 3 – D/E/F). A non-specific {NS} orientation was also tested. SEM images show that Vickers indentation tests made in {110}

orientations lead to straight cracks aligned with the diagonal of the tip, whereas tests made in {NS} and in {100} orientations show cracks slightly deviated from the targeted direction (**FIGURE 3 – D/E/F**).

Single crystal of zirconia being transparent, the use of an optical microscope permits to observe the cracks below the top surface by modifying the focus settings (**FIGURE 4**). For every studied load above 100 mN, the observed crack morphology is similar for a given crystalline orientation. These optical images show that for {110} orientations, cracks follow the targeted planes, even under the surface (**FIGURE 4-A/A'**). For {NS} and {100} orientations for all tests, a crack is clearly noted below the indentation imprint, this crack being non-visible on the top surface (**FIGURE 3**) and having an apparent orientation close to that of a {110} plane (**FIGURE 4-B/B'/C/C'**).

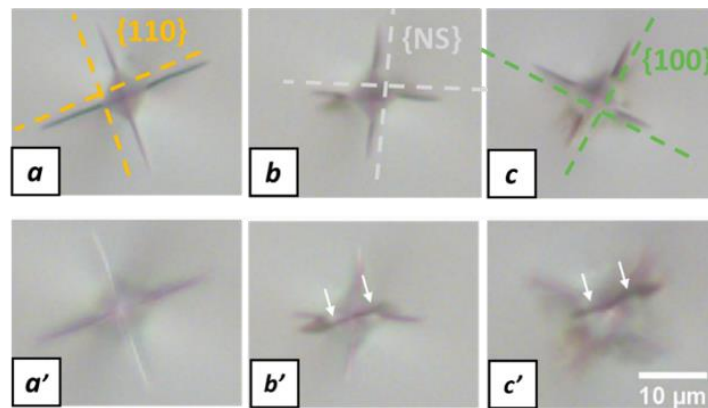


Figure 4: Optical images of Vickers indentation impressions (400 mN): (a-b-c) focusing on the sample surface; (a'-b'-c') focusing under the sample surface; for tests on {110}, {NS} (non-specific) and {100} crystalline orientations respectively. White arrows show cracks oriented in {110} planes below the surface.

For Berkovich indentation tests, only one corner of the tip can be oriented in a targeted crystalline plane, the two others being in other crystalline directions (**FIGURE 5**). Cracks in {110} planes are systematically well aligned with the diagonal of the tip and extend to the other side of the indenter (**FIGURE 5-A'**). Below the surface, cracks in {100} planes are slightly deviated from the tip axis and appear then obscured from the surface (**FIGURE 5-B'**), as the crack plane is non-perpendicular to the surface [26]. For any other direction, cracks do neither appear obscured nor crossing the residual indent.

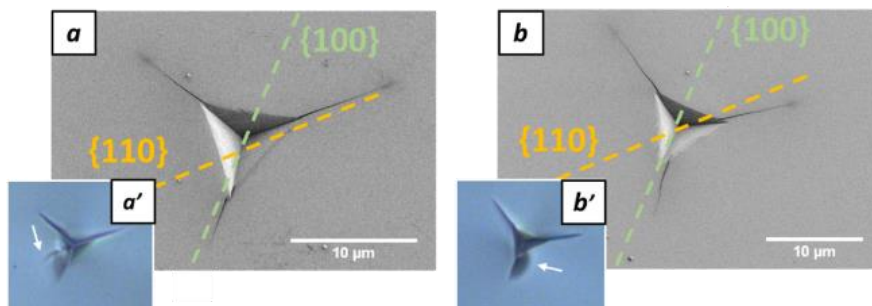


Figure 5: Residual Berkovich indentation impression on single crystal of zirconia in a {110} (a, a') and {100} orientation (b, b'): (a), (b) SEM pictures for different crystalline orientations and associated optical picture of the same impressions (a'), (b'). White arrows show (a') a long crack on {110} orientation crossing the indentation impression, (b') an obscured crack for a crack targeting {100} plane.

The length of the cracks around the imprints was measured using SEM images (**FIGURE 6**). For Vickers tests, the cracking threshold P_{th} is 100 mN for {110} and {NS} orientations and 200 mN for {100}. Berkovich tests showed that P_{th} is higher for the polycrystalline material, around 400 mN, against 100 mN for single crystal. On single crystals, the crack length c is systematically the highest for {110} orientations and the lowest for {100}, while {NS} planes are intermediate. For Berkovich tests above 400 mN, the crack length c on polycrystalline sample is lower than any tested crystalline plane of the single crystal.

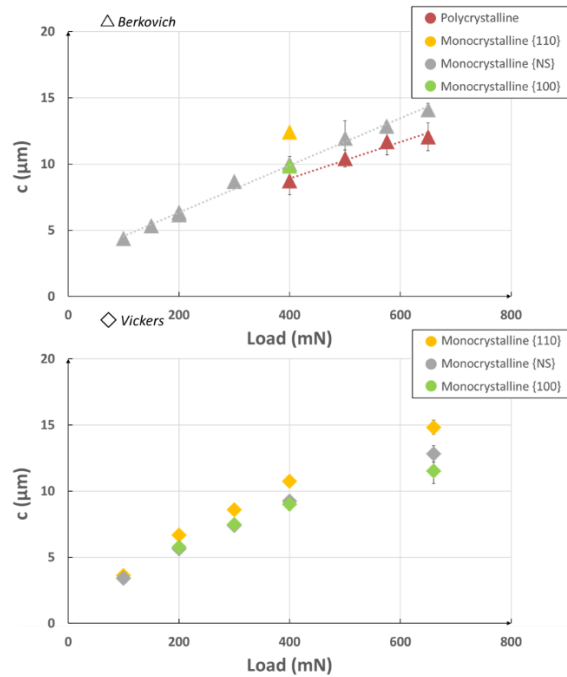


Figure 6: c parameter (see Figure 2) measured by SEM versus load applied for Berkovich (top figure) and Vickers indents (bottom figure). For each sample, the lowest load corresponds to the cracking threshold.

3.3. Hardness and indentation energy

The hardness H (**FIGURE 7**) and the irreversible energy ratio W_{irr}/W_{tot} (**FIGURE 8**) were measured over a load range from 50 mN to 650 mN including the cracking threshold load P_{th} for both Berkovich and Vickers tips.

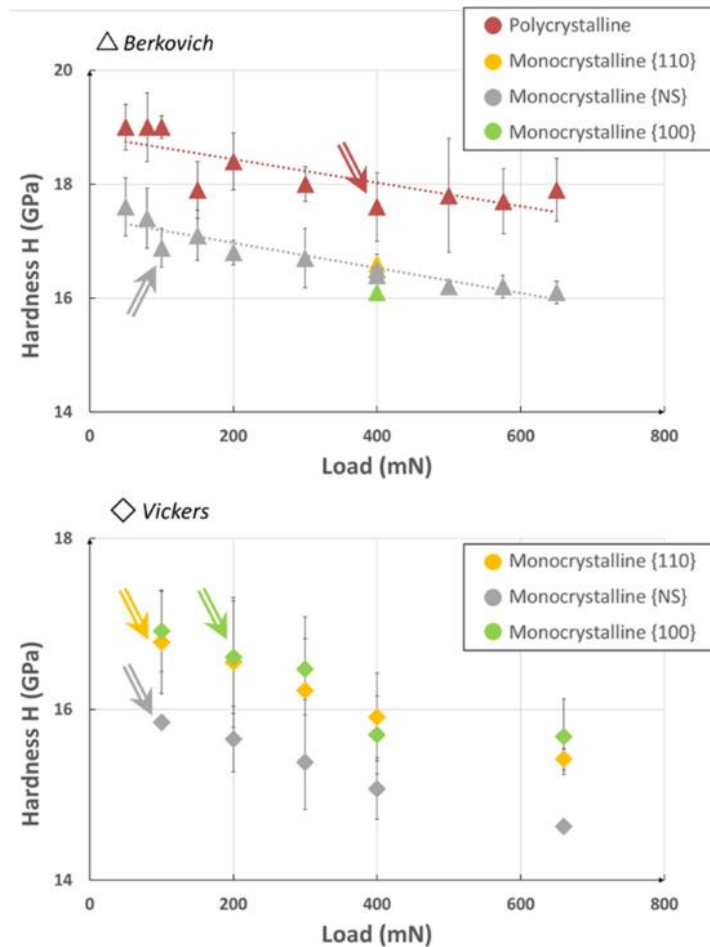


Figure 7: Hardness H against the load applied for Berkovich and Vickers indentation tests. Arrows show the data points corresponding to the cracking threshold for each tested sample.

For all configurations, the hardness diminishes with the applied load (**FIGURE 7**), decreasing to about 15% between 50 mN and 650 mN.

H measured with a Vickers tip is very close for the {110} and {100} orientations and slightly lower in the non-specific orientation {NS}. The Berkovich tests at 400 mN on the other hand show a very small difference in hardness between the tested crystalline orientations {100}, {NS} and {110}. The triangular pyramid shape of the tip is probably at the origin of this result because the diagonals of the tip stress different crystallographic directions and thus average contributions of the directions more than with a Vickers tip.

For Berkovich tests, single crystal exhibits systematically a lower hardness than the polycrystalline sample, as already noted in literature [27]. In addition, the lower Berkovich hardness in the monocrystalline sample cannot be explained by the stress of a particular direction in the crystal since it can be seen that the difference between the tested crystalline orientations is very small as measured with this tip at 400 mN.

For the Young's modulus measured at unloading, there is only little change with the applied load for the different configurations or tips used (see Appendix).

The ratio of irreversible energy W_{irr}/W_{tot} shows a global slight increase with the applied load (**FIGURE 8**). This evolution is consistent with other results obtained on ceramics [28][29], where there is a fast increase of W_{irr}/W_{tot} for low indentation loads (a few mN) before a softer growth between 50 mN and 1000 mN.

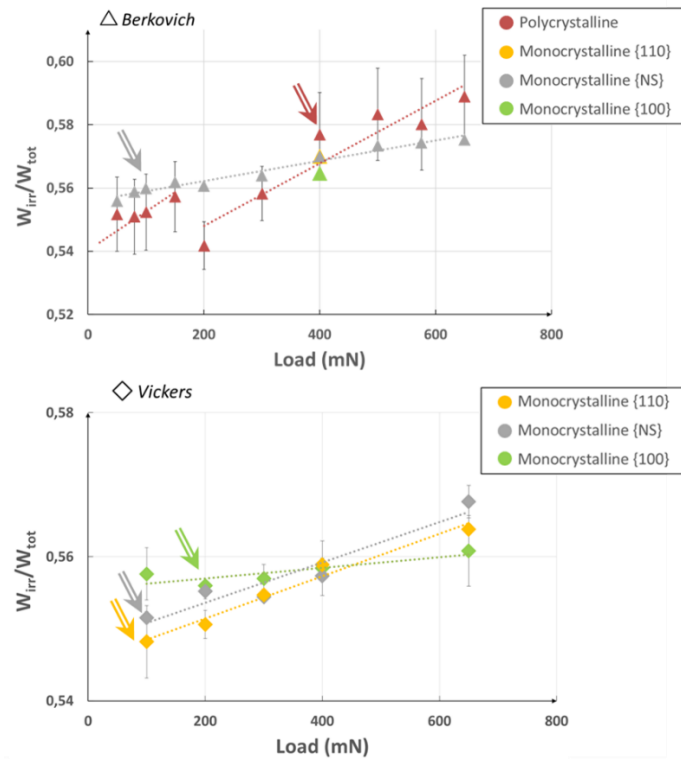


Figure 8: Ratio of irreversible indentation energy W_{irr} on the total indentation work W_{tot} against the maximum load. Arrows show the data points corresponding to the cracking threshold for each tested sample.

The monocrystalline sample tested with a Berkovich tip shows an increase of W_{irr}/W_{tot} over all the tested load range including P_{th} (50 mN for this sample). The slope of W_{irr}/W_{tot} versus the applied load is known to depend on the crystalline orientation. The polycrystalline sample tested with a Berkovich tip shows a general increase of W_{irr}/W_{tot} over the tested load range, however a break in the slope is noted between 150 mN and 200 mN load, *i.e.* below P_{th} (400 mN for this sample).

3.1. Apparent fracture toughness

Equations (2) ($\xi_R = 0.016$) and (3) ($\chi_V = 0.016$) were used to calculate the apparent fracture toughness from each Vickers and Berkovich test (**FIGURE 9**).

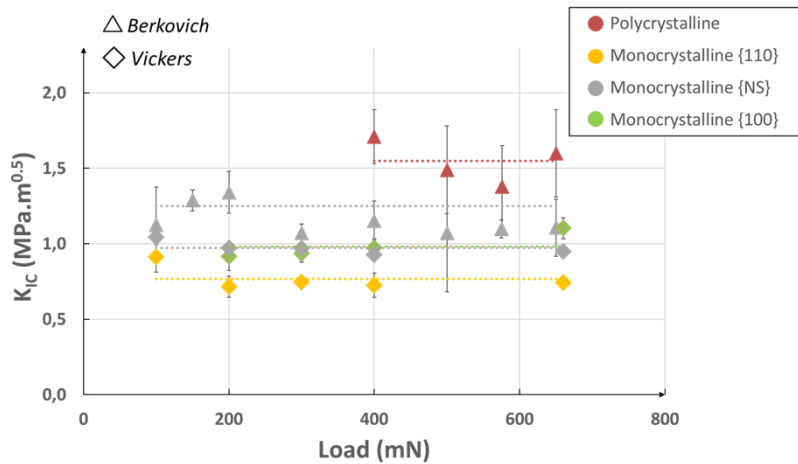


Figure 9: Apparent fracture toughness versus applied load. For each sample, the lowest load available corresponds to the cracking threshold.

It can also be seen that the toughness values are relatively stable with the applied load, despite the variation in the c/a ratio from 1.9 to 3.0 over the load range studied (see Appendix) for the Vickers tests in the {110} orientation.

4. Discussion

For both polycrystalline and monocrystalline samples, there is a progressive decrease of the hardness and an increase of the ratio of irreversible energy with applied load for both Vickers and Berkovich tests. It seems to show the presence of an indentation size effect (*ISE*). *ISE* is well known on ductile materials, especially at small penetration depths (below a few microns) [30], and is induced by a higher density of dislocations at the external surface [31]. *ISE* is also observed on ceramics, manifesting itself in a rapid decrease in hardness up to applied loads of a few mN (i.e. a sub-surface displacement of the order of a few hundred nanometers), followed by a much slower decrease [29]. This is consistent with the evolution of the hardness observed in this work (**FIGURE 7**). The sources of *ISE* are related to constrained plasticity effects as for metallic materials, even if these sources are not precisely known [32]. A decrease in hardness with increasing load is also observed on ceramics at much higher loads and displacements [33], up to forces of 50 N [11]. This phenomena could be due to a progressive cracking during the indentation test; the greater the applied load, the longer and the more numerous the cracks generated and the lower the apparent hardness [11].

Comparison of polycrystalline and monocrystalline samples illustrates the influence of grain boundaries on hardness, with a larger hardness for the polycrystalline sample (**FIGURE 7**). The increase of hardness due to the presence of grain boundaries appears to be constant in all the load range tested. In our study, for the lowest applied loads, the size of plastically deformed zone during indentation has a size close to or greater than grain size. Indeed, the size of the affected area around an imprint is typically a few times the length of Vickers diagonal, i.e., up to 20 times the penetration depth. For tests at 100 mN, the maximum penetration depth h is around 500 nm (**FIGURE 2**), leading to a size of affected area around 10 μm while the average grain size is $6.5 \pm 3.1 \mu\text{m}$. This suggests that in the load range used, grain boundaries influence hardness: grain boundaries probably block

dislocations, resulting in a higher apparent hardness, as already noted in microhardness tests on polycrystalline metals and ceramics [34][35].

Regarding the influence of indentation induced cracking in the present work, the evolution in hardness and in energy ratio with the applied load seem unaffected by the cracking threshold load P_{th} (**FIGURE 7**). This supports that a limited amount of energy is dissipated during cracking as compared to that dissipated in plastic deformation.

The Vickers tip creates a chaotic crack system far from the model case, *i.e.* a single crack starting from each corner of the indentation impression. Berkovich tests are more satisfactory in terms of crack morphology, but still, the crack pattern is not as well defined as in the monocrystalline sample (**FIGURE 3**). On the polycrystalline sample, crack patterns appears to be influenced by the local microstructure. It is potentially because for such applied loads, the size of the residual indentation impression is close or larger than the grain size ($6.5 \pm 3.1 \mu\text{m}$).

For the single crystal, there is a clear influence of the crystalline orientation on the generated cracks. Both Vickers (**FIGURE 3**) and Berkovich tests (**FIGURE 4**) showed that the {110} plan seems to be systematically preferred for the crack propagation: cracks seen from the surface are longer and are always well aligned with the impression diagonals (**FIGURE 3** and **FIGURE 5**). In contrast, for {100} and {NS} orientations, a crack is visible under Vickers impressions and follows a {110} plane (**FIGURE 4**). Hence, cracks seem to deviate towards {110} planes, as already observed on single crystals of cubic zirconia [26].

The calculated fracture toughness appears to largely depend on the equation used (**TABLE 1**). The fracture toughness calculated by the Anstis equation (Vickers tip) is far from the literature values: they are about twice as low. On the other hand, the Dukino equation (Berkovich tip) gives very similar results, showing that this formula is particularly well adapted to the material of this study (**TABLE 1** *ERREUR ! SOURCE DU RENVOI INTROUVABLE.*). The observed differences with the equations from literature may be partly related to the relatively low c/a ratios in this paper, as compared to values in the literature [20]. Usually, it is common to look for situations where the c/a ratio exceeds 2 to have well developed cracks. Also, depending on the value of c/a , different cracking modes are commonly assumed, a M mode for $c/a > 2.5$ and a P mode when $c/a < 3.5$ [25]. Thus, for values of c/a close to 2-2.5, as it is the case in this paper, we are in a c/a range where the cracks are short and the cracking modes not straightforward to define. This points out the importance of calibration for reliable indentation toughness measurements.

For the single crystal in a non-specific crystalline orientation, fracture toughness is relatively different between the Vickers tip ($0.96 \pm 0.02 \text{ MPa.m}^{0.5}$) and the Berkovich tip ($1.16 \pm 0.10 \text{ MPa.m}^{0.5}$). This difference in toughness originates probably from the choice of different pre-factors taken for the fracture toughness equation.

Table 1 : Apparent fracture toughness (averaged on the studied load range) results obtained with (Vickers) equation (2) and (Berkovich) equation (3) on different samples and sample orientations. Comparison with literature values.

Sample	K_{IC} (MPa.m ^{0.5}) mean value ± standard deviation				
	This work		Comparison with literature		
	Vickers tip Anstis eq. [20]	Berkovich tip Dukino eq. [22]	SENB [36]	SENB [37]	μcantilever [38]
Mono. {100}	0.98 ± 0.08	-	1.9 ± 0.1	-	1.41 ± 0.19
Mono. {NS}	0.96 ± 0.02	1.16 ± 0.10	-	-	-
Mono. {110}	0.73 ± 0.01	-	1.48 ± 0.04	-	1.61 ± 0.05
Mono. {111}	-	-	-	-	1.44 ± 0.15
Polycrystalline	-	1.54 ± 0.14	-	1.54 ± 0.05	-

The apparent fracture toughness of polycrystalline and monocrystalline cubic zirconia can be compared using Berkovich tests. The results are in good agreement with the literature value ($K_{IC} = 1.54$ MPa.m^{0.5}), while the single crystal appears to be less tough ($K_{IC} = 1.16$ MPa.m^{0.5}). This confirms quantitatively the conclusion drawn previously by the crack size measurement around indentation impressions: the presence of multiple grains increases the apparent fracture toughness.

From Vickers oriented tests, the apparent fracture toughness for {110} planes is 0.73 MPa.m^{0.5} against around 1.0 MPa.m^{0.5} for the {100} orientation, this tendency being very reproducible for different applied loads above the threshold value. The evolution in fracture toughness with the applied load (**FIGURE 9**) is mainly controlled by the crack length (**FIGURE 6**), this parameter appearing as the most dominant in the equations. It is the expected order of plane resistance in this cubic crystal, where {110} planes are less resistant than {100} planes [36]. However, the important variation of the cracking system with crystalline orientation (as illustrated in **FIGURE 4**) leads possibly to a misjudged crack area, and thus to a misjudged fracture toughness, as already mentioned by Pajares *et al.* [26].

A deviation of the cracking system from the theoretical case is also observed for Berkovich test in the monocrystalline sample, when a diagonal of the imprint is aligned towards a {100} plane, the generated cracks deviate slightly towards a {110} plane, but not entirely (**FIGURE 5**). This could be related to a lower toughness for {110} planes. In addition, the elastic anisotropy of the crystal also affects the cracking process. Possibly, it can play a role in the observed partial crack deviation to {110} planes. The large difference of rigidity between <100> (approx. 360 GPa for cubic zirconia) and <110> directions (approx. 185 GPa) could lead to a complex stress distribution around the indent, and thus to an anisotropic cracking system [39]. Finally, the strong elastic anisotropy of the crystal questions the fracture toughness determination by indentation testing : the evaluation of toughness is not straightforward because of the complex stress distribution [8], particularly in the case of an anisotropic material.

The lower toughness value of {110} planes, even if expected for a cubic crystal, is in contradiction with bending tests on FIB-milled microcantilevers inside cubic zirconia grains [38]. In these micro-bending tests, no significant differences were noted on the fracture toughness of the three crystallographic families of planes {100}, {110} and {111} with values ranging from 1.4 to 1.6 MPa.m^{1/2} on the very same zirconia sample as in this work, with the same surface preparation. This difference could be due to different reasons. FIB milling could lead to ion implantation and amorphization at the bottom of the indentation, possibly averaging the values between the different planes tested. Indentation is also based on a crack arrest criterion, while bending is based on a propagation criterion. Finally, the stress mode is uni-directional for bending, whereas it is three-dimensional for indentation, on a material that is anisotropic.

5. Conclusion

- In polycrystalline zirconia, for applied loads generating an indentation impression about the size of a single grain, the Vickers tip leads to multiple and chaotic cracking, while the Berkovich tip leads to a better-defined surface cracking.
- Vickers and Berkovich tests show an indentation size effect, noted on both the hardness H and on the irreversible on total indentation energy ratio W_{irr}/W_{tot} , but not on the Young's modulus E . This ISE can be related to constrained plasticity effects at low loads and to cracking at higher loads. No obvious link between the cracking threshold load and the evolution of H or W_{irr}/W_{tot} versus applied load was possible. The energy dissipated during the fracture process is therefore difficult to extract from the energies involved during indentation.
- For monocrystalline samples, there is a clear dependence of the cracking system under the indent and at the surface with the crystalline orientation. The {110} type plane corresponds to the most favorable for crack propagation as expected for a cubic crystal.
- The Berkovich tip averages the fracture toughness in different crystal orientations due to the triangular impression geometry. However, crack deviation towards the {110} planes is noted.
- In order to evaluate the apparent fracture toughness by the indentation method in anisotropic cases (single crystals or inside the grains of a polycrystalline sample), it is necessary to carefully analyze the crack pattern regarding the model used for the determination of fracture toughness, as well as to check if the equation and the calibration values are adapted to the material under study.

Acknowledgements

This research project was mainly funded by CEA and INSA-Lyon, and was also financially supported by EDF and Framatome.

Bibliography

- [1] H. Hertz, *Hertz's Miscellaneous Papers*. 1896.
- [2] B. R. Lawn, "Indentation of Ceramics with Spheres : A century After Hertz," *J. Am. Ceram. Soc.*, vol. 81, no. 8, pp. 1977–94, 1998.
- [3] B. Lawn and R. F. Cook, "Probing Material Properties with Sharp Indenters : A Restrospective," *J. Mater. Sci.*, vol. 47, no. 1, pp. 1–22, 2012.
- [4] D. B. Marshall *et al.*, "The Compelling Case for Indentation as a Functional Exploratory and Characterization Tool," *J. Am. Ceram. Soc.*, vol. 98, no. 9, pp. 2671–2680, 2015, doi: 10.1111/jace.13729.
- [5] D. M. Marsh, "Plastic Flow and Fracture in Glass," *Proce. Roy. Soc. Lond.*, vol. 282, no. 1388, pp. 33–43, 1964.
- [6] Palmqvist, "Method att Bestamma Segheten hos Spread Material, Sarskit Hardmettaler," *Jernkontorets Ann.*, pp. 141–146, 1957.
- [7] A. G. Evans and E. A. Charles, "Fracture toughness Determination by Indentation," *J. Am. Ceram. Soc.*, vol. 59, no. 7–8, pp. 371–2, 1976.
- [8] G. D. Quinn and R. C. Bradt, "On the vickers indentation fracture toughness Test," *J. Am. Ceram. Soc.*, vol. 90, no. 3, pp. 673–680, 2007, doi: 10.1111/j.1551-2916.2006.01482.x.
- [9] J. M. Gatt, J. Sercombe, I. Aubrun, and J. C. Ménard, "Experimental and numerical study of fracture mechanisms in UO₂ nuclear fuel," *Eng. Fail. Anal.*, vol. 47, pp. 299–311, 2015, doi: 10.1016/j.engfailanal.2014.07.019.
- [10] D. Di Maio and S. G. Roberts, "Measuring fracture toughness of coatings using focused-ion-beam-machined microbeams," *J. Mater. Res.*, vol. 20, no. 02, pp. 299–302, 2005, [Online]. Available: http://www.journals.cambridge.org/abstract_S0884291400084016.
- [11] J. B. Quinn and G. D. Quinn, "Indentation brittleness of ceramics : a fresh approach," *J. Mater. Sci.*, vol. 2, pp. 4331–4346, 1997.
- [12] F. Petit, V. Vandeneede, and F. Cambier, "Relevance of instrumented micro-indentation for the assessment of hardness and Young's modulus of brittle materials," *Mater. Sci. Eng. A*, vol. 456, no. 1–2, pp. 252–260, 2007, doi: 10.1016/j.msea.2006.11.109.
- [13] C. Ullner, "Instrumented indentation test for advanced technical ceramics," *J. Eur. Ceram. Soc.*, vol. 22, pp. 1183–1189, 2002.
- [14] W. C. Oliver and G. M. Pharr, "An improved technique for determining hardness and elastic modulus using load and displacement sensing indentation experiments," *J. Mater. Res.*, vol. 7, no. 6, pp. 1564–

- 1583, 1992.
- [15] R. F. Cook and G. M. Pharr, "Direct observation and analysis of indentation cracking in glasses and ceramics," *J. Am. Ceram. Soc.*, vol. 73, no. 4, pp. 787–817, 1990.
- [16] A. Iost, "Détermination de la ténacité de matériaux fragiles ou ductiles à partir de l'essai d'indentation," *Rev. Metall. Cah. D'Informations Tech.*, vol. 110, no. 3, pp. 215–233, 2013, doi: 10.1051/metal/2013065.
- [17] C. B. Ponton and R. D. Rawlings, "Vickers indentation fracture toughness test Part 1 Review of literature and formulation of standardised indentation toughness equations," *Mater. Sci. Technol.*, vol. 5, pp. 865–871, 1989.
- [18] C. B. Ponton and R. D. Rawlings, "Vickers indentation fracture toughness test Part 2 Review of literature and formulation of standardised indentation toughness equations," *Mater. Sci. Technol.*, vol. 5, pp. 961–975, 1989.
- [19] B. R. Lawn, A. G. Evans, and D. B. Marshall, "Elastic/Plastic Indentation Damage in Ceramics : The Median/Radial Crack System," *J. Am. Ceram. Soc.*, vol. 63, p. 574, 1980.
- [20] G. R. Anstis *et al.*, "A Critical Evaluation of Indentation Techniques for Measuring Fracture Toughness: I, Direct Crack Measurements," *J. Am. Ceram. Soc.*, vol. 64, no. 9, pp. 533–538, 1981, doi: 10.1111/j.1151-2916.1981.tb10320.x.
- [21] M. T. Laugier, "New Formula ofr indentation toughness in ceramics," *J. Mater. Sci. Lett.*, vol. 6, pp. 355–356, 1987.
- [22] R. D. Dukino and M. V. Swain, "Comparative Measurement of Indentation Fracture Toughness with Berkovich and Vickers Indenters," *J. Am. Ceram. Soc.*, vol. 75, no. 12, pp. 3299–3304, 1992, doi: 10.1111/j.1151-2916.1992.tb04425.x.
- [23] N. Cuadrado, D. Casellas, M. Anglada, and E. Jiménez-Piqué, "Evaluation of fracture toughness of small volumes by means of cube-corner nanoindentation," *Scr. Mater.*, vol. 66, no. 9, pp. 670–673, 2012, doi: 10.1016/j.scriptamat.2012.01.033.
- [24] M. He, F. Li, J. Cai, and B. Chen, "An indentation technique for estimating the energy density as fracture toughness with Berkovich indenter for ductile bulk materials," *Theor. Appl. Fract. Mech.*, vol. 56, no. 2, pp. 104–111, 2011, doi: 10.1016/j.tafmec.2011.10.006.
- [25] M. T. Laugier, "Palmqvist toughness in WC-Co composites viewed as a ductile/brittle transition," *J. Mater. Sci. Lett.*, vol. 6, pp. 768–770, 1987.
- [26] A. Pajares, F. Guiberteau, A. Dominguez-rodriguez, and A. H. Heuer, "Indentation-induced cracks and the toughness anisotropy of 9.4-mol%-yttria-stabilized cubi zirconia single crystals," *J. Am. Ceram. Soc.*, vol. 62, pp. 859–862, 1991.

- [27] K. Kurosaki, D. Setoyama, J. Matsunaga, and S. Yamanaka, "Nanoindentation tests for TiO₂, MgO, and YSZ single crystals," *J. Alloys Compd.*, vol. 386, no. 2005, pp. 261–264, 2005, doi: 10.1016/j.jallcom.2004.05.016.
- [28] B. K. Jang, "Influence of low indentation load on Young's modulus and hardness of 4 mol% Y₂O₃-ZrO₂ by nanoindentation," *J. Alloys Compd.*, vol. 426, no. 1–2, pp. 312–315, 2006, doi: 10.1016/j.jallcom.2006.01.086.
- [29] P. Maiti, M. Bhattacharya, P. S. Das, P. S. Devi, and A. K. Mukhopadhyay, "Indentation size effect and energy balance issues in nanomechanical behavior of ZTA ceramics," *Ceram. Int.*, vol. 44, no. 8, pp. 9753–9772, 2018, doi: 10.1016/j.ceramint.2018.02.210.
- [30] B. R. Lawn and R. F. Cook, "Probing material properties with sharp indenters: A retrospective," *J. Mater. Sci.*, vol. 47, no. 1, pp. 1–22, 2012, doi: 10.1007/s10853-011-5865-1.
- [31] W. D. Nix and H. Gao, "Indentation size effects in crystalline materials: a law for strain gradient plasticity," *J. Mech. Phys. Solids*, vol. 46, no. 3, 1998.
- [32] S. Koizumi, T. Hiraga, and T. S. Suzuki, "Vickers indentation tests on olivine: size effects," *Phys. Chem. Miner.*, vol. 47, no. 2, pp. 1–14, 2020, doi: 10.1007/s00269-019-01075-5.
- [33] J. Gong, J. Wu, and Z. Guan, "Examination of the indentation size effect in low-load vickers hardness testing of ceramics," *J. Eur. Ceram. Soc.*, vol. 19, no. 15, pp. 2625–2631, 1999, doi: 10.1016/S0955-2219(99)00043-6.
- [34] A. Krell and S. Schädlich, "Nanoindentation hardness of submicrometer alumina ceramics," *Mater. Sci. Eng. A*, vol. 307, no. 1–2, pp. 172–181, 2001, doi: 10.1016/S0921-5093(00)01818-9.
- [35] I. Manika and J. Maniks, "Size effects in micro- and nanoscale indentation," *Acta Mater.*, vol. 54, no. 8, pp. 2049–2056, 2006, doi: 10.1016/j.actamat.2005.12.031.
- [36] A. Pajares and F. Guiberteau, "Microhardness and Fracture Toughness Anisotropy in Cubic Zirconium Oxide Single Crystals," *J. Am. Ceram. Soc.*, vol. 71, no. 7, pp. 332–333, 1988, doi: 10.1111/j.1151-2916.1988.tb05933.x.
- [37] R. A. Cutler, J. R. Reynolds, and A. Jones, "Sintering and Characterization of Polycrystalline Monoclinic, Tetragonal, and Cubic Zirconia," *J. Am. Ceram. Soc.*, vol. 75, no. 8, pp. 2173–2183, 1992, doi: 10.1111/j.1151-2916.1992.tb04480.x.
- [38] R. Henry *et al.*, "Local fracture toughness measurements in polycrystalline cubic zirconia using micro-cantilever bending tests," *Mech. Mater.*, vol. 136, Sep. 2019, doi: 10.1016/j.mechmat.2019.103086.
- [39] J. D. Stanescu and H. M. Chan, "Indentation study of fracture toughness anisotropy in cubic zirconium oxide single crystals," *J. Mater. Sci. Lett.*, vol. 11, pp. 1364–1365, 1992.

Appendix

Indentation parameters measured for Berkovich tests on monocrystalline sample.

Berkovich - Monocrystalline sample						
Orient.	P (mN)	H (GPa)	E (GPa)	c (μm)	$W_{\text{irr}}/W_{\text{tot}}$	c/a
{NS}	50	17.6 \pm 0.51	258 \pm 15	-	0.556 \pm 0.004	-
{NS}	80	17.4 \pm 0.53	259 \pm 5	-	0.559 \pm 0.001	-
{NS}	100	16.9 \pm 0.34	245 \pm 10	4.36 \pm 0.30	0.560 \pm 0.003	1.86 \pm 0.15
{NS}	150	17.1 \pm 0.44	256 \pm 7	5.32 \pm 0.09	0.562 \pm 0.001	1.85 \pm 0.06
{NS}	200	16.8 \pm 0.22	254 \pm 2	6.16 \pm 0.39	0.566 \pm 0.001	1.91 \pm 0.16
{NS}	300	16.7 \pm 0.52	245 \pm 3	8.68 \pm 0.25	0.564 \pm 0.001	2.10 \pm 0.18
{NS}	400	16.4 \pm 0.10	254 \pm 2	10.00 \pm 0.11	0.567 \pm 0.002	2.19 \pm 0.08
{100}	400	16.1 \pm 0.02	259 \pm 16	9.84 \pm 0.74	0.565 \pm 0.006	2.00 \pm 0.17
{110}	400	16.6 \pm 0.17	249 \pm 14	12.41 \pm 0.32	0.570 \pm 0.004	2.55 \pm 0.10
{NS}	500	16.2 \pm 0.10	256 \pm 3	11.93 \pm 1.34	0.573 \pm 0.003	2.30 \pm 0.32
{NS}	575	16.2 \pm 0.20	259 \pm 2	12.86 \pm 0.32	0.574 \pm 0.004	2.33 \pm 0.08
{NS}	650	16.1 \pm 0.20	259 \pm 4	14.10 \pm 0.48	0.575 \pm 0.001	2.28 \pm 0.29

Indentation parameters measured for Berkovich tests on polycrystalline sample.

Berkovich - Polycrystalline sample						
Orient.	P (mN)	H (GPa)	E (GPa)	c (μm)	$W_{\text{irr}}/W_{\text{tot}}$	c/a
-	50	19.0 \pm 0.6	266.9 \pm 3.2	-	0.552 \pm 0.012	-
-	80	19.0 \pm 0.2	268.1 \pm 4.9	-	0.551 \pm 0.012	-
-	100	19.0 \pm 0.5	272.2 \pm 6.3	-	0.552 \pm 0.011	-
-	150	17.9 \pm 0.5	265 \pm 5.3	-	0.557 \pm 0.007	-
-	200	18.4 \pm 0.3	260.4 \pm 4.9	-	0.542 \pm 0.009	-
-	300	18.0 \pm 0.6	265.6 \pm 2.9	-	0.558 \pm 0.013	-
-	400	17.6 \pm 1.0	273.8 \pm 9.5	8.7 \pm 1	0.577 \pm 0.015	1.83 \pm 0.27
-	500	17.8 \pm 0.6	265 \pm 11.3	10.4 \pm 0.7	0.583 \pm 0.014	1.94 \pm 0.15
-	576	17.7 \pm 0.6	263.4 \pm 12.5	11.7 \pm 1	0.580 \pm 0.013	2.02 \pm 0.22
-	650	17.9 \pm 0.6	280.8 \pm 16.5	12 \pm 1.1	0.589 \pm 0.012	1.96 \pm 0.21

Indentation parameters measured for Vickers tests on monocrystalline sample.

Vickers - Monocrystalline sample						
Orient.	P (mN)	H (GPa)	E (GPa)	c (μm)	W _{irr} /W _{tot}	c/a
{110}	100	16.8 ± 0.6	255.4 ± 1.6	3.6 ± 0.1	0.537 ± 0.003	1.92 ± 0.10
{110}	200	16.6 ± 0.8	250 ± 4.7	6.7 ± 0.3	0.553 ± 0.004	2.42 ± 0.31
{110}	300	16.2 ± 0.9	250 ± 6.2	8.6 ± 0.3	0.557 ± 0.004	2.59 ± 0.17
{110}	400	15.9 ± 0.5	250 ± 3.7	10.7 ± 0.1	0.555 ± 0.007	2.80 ± 0.09
{110}	660	15.4 ± 0.1	246.7 ± 5.6	14.8 ± 0.5	0.547 ± 0.001	2.99 ± 0.14
{100}	100	16.9 ± 0.5	273.8 ± 0.4	-	0.551 ± 0.001	-
{100}	200	16.6 ± 0.7	265 ± 4.6	5.8 ± 0.2	0.597 ± 0.012	2.13 ± 0.12
{100}	300	16.5 ± 0.4	265 ± 3.3	7.5 ± 0.2	0.580 ± 0.008	2.23 ± 0.08
{100}	400	15.7 ± 0.5	265 ± 2.5	9 ± 0.2	0.565 ± 0.004	2.36 ± 0.08
{100}	660	15.7 ± 0.4	261.1 ± 2.2	11.5 ± 0.9	0.553 ± 0.002	2.31 ± 0.23
{NS}	100	15.8 ± 0.1	264.6 ± 2.5	3.4 ± 0	0.542 ± 0.002	1.83 ± 0.03
{NS}	200	15.7 ± 0.4	255 ± 4.3	5.6 ± 0.1	0.552 ± 0.003	2.16 ± 0.09
{NS}	300	15.4 ± 0.6	255 ± 4.4	7.4 ± 0.1	0.574 ± 0.006	2.28 ± 0.03
{NS}	400	15.1 ± 0.4	255 ± 8.8	9.3 ± 0.3	0.609 ± 0.048	2.47 ± 0.17
{NS}	660	14.6 ± 0.1	247.9 ± 0.9	12.8 ± 0.6	0.555 ± 0.002	2.61 ± 0.16